Seismic Behavior of CFT Column and Steel Pile Footings

Yan Xiao, M.ASCE[1]; Zhongxin Zhang[2]; Jianhua Hu[3]; Sashi K. Kunnath, F.ASCE[4]; and Pengxin Guo[5]

Abstract: In this study, two column and pile-footing models consisting of concrete-filled steel tube (CFT) columns, reinforced concrete footings, and steel H-piles were designed and constructed at approximately one-fifth scale. The experimental differences between the two models were in the design details of the CFT column-to-footing connections. One connection consisted of welded studs, and the other used a base plate and stiffeners. The two models were tested in a vertical cantilever condition with cyclic horizontal forces and a constant axial load applied to the top of the column. The model footings were supported on 16 model steel H-piles simulating the pile foundation. Under imposed horizontal displacement, the two models with different CFT-to-pile-cap connection details demonstrated satisfactory cyclic behavior, with the development of full plastic hinges at the bottom of the columns. Strut-and-tie modeling analysis was carried out to show the force-resisting mechanism in the reinforced concrete footing. The study also validated a new design detail for the anchorage of steel H-piles to pile caps.
DOI: 10.1061/(ASCE)BE.1943-5592.0000198.

CE Database subject headings: Bridges; Columns; Footings; Seismic design; Piles.

Author keywords: Bridges; Concrete-filled tubes (CFT); Columns; Pile footing; Steel H-piles; Seismic design; Strut-and-tie model.

Introduction

Extensive investigations have been carried out on concrete-filled steel tube (CFT) members during the last two decades, and the constructional merits of CFT members are widely recognized. In a CFT column, the steel tube enhances the shear resistance and confines the concrete core, therefore increasing the compressive strain capacity of the concrete and displacement ductility. In addition to providing increased flexural stiffness and compressive resistance, the concrete infill restrains or delays local buckling of the tube. Other than serving as reinforcement, the steel tubes also serve as formwork, reducing the labor and material cost required for construction. Although CFT members offer significant structural and constructional benefits, their connections to foundations are typically complicated. In bridges, the loads from the superstructure must be transferred down through the substructure to the footing and into the piles. Because of the importance of the base connection of the columns, a robust base connection is required for reliable CFT construction.

Although a significant number of CFT tests have been conducted, there have been far fewer tests on CFT connections, particularly column-footing connections. Existing details for column base connections can be divided into the following categories: (1) exposed base-plate connection, (2) embedded connection, (3) structural steel connection, (4) transfer bar connection, (5) semi-embedded connection, (6) embedded with annular ring connection, and (7) fully embedded with or without stiffeners connection. These connections may develop the flexural strength of the composite CFT column section and cyclic drift capacity of the footing, but they are not necessarily cost effective. To simplify the construction and reduce the cost, two different embedded connections, one using a base plate and stiffeners and the other using welded studs, were tested in this research.

A base-plate connection, in which a base plate is attached to the pile footing with bolts embedded into the footing in advance, is convenient for construction and has been implemented in design (Hitaka et al. 2003). However, base plates were found to be seriously damaged during the Kobe earthquake because of limited rotational stiffness and partially fixed end conditions. For this reason, a new model of bearing-type CFT column base connection enhanced with reinforcing steel transfer was proposed and investigated (Kadoya et al. 2005) and was shown to provide enhanced strength and drift footing capacity. However, the use of reinforcing transfer steel increased the difficulty of construction and project cost. Compared with bearing-type connections, embedded-type connections are more effectively guarantee adequate strength of the connection to allow the development of the column yielding. Marson and Bruneau (2004) used a pair of embedded steel channels to connect the steel tube to the pile footing, neglecting the need for reinforcing steel in the pile footing. Hsu and Lin (2003) tested rectangular CFT columns with embedment depths equal to 0.5, 1.0, and 1.5 times the column dimension, D, with a full rectangular base plate welded to the base as anchorage. It was demonstrated that the model column with an embedment depth of $1.0D$ could achieve the theoretical flexural strength and large drifts with minimal damage to the foundation, but premature

[1]Director, Ministry of Education Key Laboratory of Building Safety and Energy Efficiency, Center for Integrated Protection Research of Engineering Structures, Hunan Univ., Changsha, Hunan 410082, China; and Professor, Dept. of Civil Engineering, Univ. of Southern California, Los Angeles, CA 90089-2531 (corresponding author). E-mail: yanxiao@usc.edu

[2]Henan Electric Power Survey and Design Institute, Zhengzhou 450007, China; formerly, Research Assistant, Center for Integrated Protection Research of Engineering Structures, College of Civil Engineering, Hunan Univ., Changsha, Hunan 410082, China.

[3]Hunan Province Communication Planning Survey and Design Institute, Changsha 410008, China.

[4]Professor, Dept. of Civil Engineering, Univ. of California, Davis, CA 95616. E-mail: skkunnath@ucdavis.edu

[5]Research Assistant, Center for Integrated Protection Research of Engineering Structures, College of Civil Engineering, Hunan Univ., Changsha, Hunan 410082, China.

Note. This manuscript was submitted on February 2, 2010; approved on November 17, 2010; published online on August 15, 2011. Discussion period open until February 1, 2012; separate discussions must be submitted for individual papers. This paper is part of the ***Journal of Bridge Engineering***, Vol. 16, No. 5, September 1, 2011. ©ASCE, ISSN 1084-0702/2011/5-575–586/$25.00.

cracking in the base concrete occurred before yielding of the CFT column with an embedment depth of $0.5D$. An embedment depth greater than $1.0D$ offered little improvement in the behavior of the model. Kingsley et al. (2005) tested three specimens using embedded connections to evaluate the influence of the embedded length and footing vertical shear reinforcement on the response of the connection. Kingsley et al. adopted an annular base plate in the study, which improved the condition of the concrete under the column base plate.

Bridge footing design following most current design provisions is essentially based on a capacity design approach utilizing the column's ultimate flexural moment, shear, and axial force with proper consideration of overstrength to determine the required flexural and shear strength of the pile cap and the capacity of the piles. However, the design for flexure and shear of footings based on a one-way beam model lacks experimental verification. In addition, there is a lack of rational consideration of column-footing joint shear in current design. Tests and supporting analyses by Xiao et al. (1999) on a 1:2.5 scale reinforced concrete circular-column footing model revealed that the flexural and shear design of the column-footing connection based on full effectiveness of the entire footing width is nonconservative. Xiao et al.'s study on

Table 1. Details of Prototype Column Footings

Bent	Column diameter and reinforcement	Piles	Footing $L_f \times B_f \times T_f$ (m)	Footing top reinforcement	Footing bottom reinforcement	Footing stirrups
Bent-2	2.13 m; 54 #43 bars[a]	25-100T	$7 \times 7 \times 1.75$	19 #32 both directions	37 #32 both directions	200 #16 J-bars
Bent-3	2.13 m; 36 #57 bars	30-100T	$8.5 \times 7.6 \times 1.92$	26 #32 longitudinal 25 #32 transverse	51 #32 longitudinal 49 #32 transverse	310 #16 J-bars
Bent-4	2.13 m; 64 #57 bars and 30 #36 bars	30-100T	$9.3 \times 8.5 \times 1.92$	33 #32 longitudinal 34 #32 transverse	65 #32 longitudinal 67 #32 transverse	464 #16 J-bars
Bent-5	1.68 m; 33 #57 bars	24-100T	$7 \times 6.4 \times 1.92$	7 #25 both directions	45 #25 both directions	336 #16 J-bars
Bent-6	1.68 m; 22 #36 bars and 22 #57 bars	20-100T	$7 \times 6.4 \times 1.75$	24 #25 both directions	47 #25 both directions	324 #16 J-bars

[a]Designation of bar size: #43 implies 43-mm nominal bar diameter.

Fig. 1. Steel tube base details: (a) stiffened end plate; (b) studs (images by the authors)

column footing connections (Xiao et al. 1996, 1999) is extended in this research to develop improved design procedures for CFT column-footing design.

Steel H-piles are applicable for conditions in which the soil is not capable of preventing buckling of the piles. Such conditions occur for soil types such as liquefiable sands and bay mud, and piles used in such soil types should be designed as unbraced columns (Mays and Hill 2006). Steel H-piles in Mays and Hill's research were designed as unbraced columns, without lateral restrictions from soils, to simulate pile foundation used in fluid soils due to high seismicity. To ensure the plastic hinge development of H-piles before the cap concrete reaches its capacity, Shama et al. (2002) provided some guidelines for the required embedded length of the H-piles and retrofit of H-piles to concrete cap connections. Xiao et al.'s experimental studies (2006) showed that although the pile-to-pile-footing connection was designed as a pinned connection following typical design practice in most western states in the United States, the connection can still sustain a significant amount of moment, which may cause unexpected cracking and failure in the pile cap. Test results also indicated that the anchorage details using conventional two V-shaped bars could not develop the full design ultimate tensile capacity of a pile (Xiao et al. 2006). Welding anchor bars to the H-piles is therefore investigated in this project to improve the anchorage of the pile into the pile footing.

Experimental Program

Prototype Bridge

A bridge in California named the Russian River Bridge in the San Francisco Bay Area selected for a previous study (Xiao et al. 1999) from more than 100 candidate bridges was used as the prototype for designing the testing model in this study. The bridge was a three-lane traffic single-column bent bridge and was built in 1982. The bridge has five single-column bents and two abutments at the ends. Dimensions and reinforcement details for each single-column bent are shown in Table 1. Bent-2, which has a superimposed axial load of 10,230 kN and a column longitudinal steel ratio of 2.2% of the gross sectional area, was selected as the prototype column for the model testing. The CFT model column design was based on the equivalent ultimate flexural strength of the prototype pier of Bent-2, shown in Table 1.

Bridge Column Pile-Footing Model

A CFT column with the equivalent ultimate flexural strength of the prototype reinforcement pier was obtained, and the corresponding full-scale bridge column pile-footing model was determined. Two experimental models were then designed to represent one-fifth scale of the prototype. According to previous research, one of the key issues in CFT column-to-footing connection is ensuring the force transfer of the steel tube to the foundation. To achieve this, a relatively narrow end ring plate and studs were considered in this project for specimens BCPF-1 and BCPF-2, respectively, as exhibited in Figs. 1 and 2. As shown in Fig. 2, the steel tubes were 360 mm in diameter and 6 mm thick, constituting a diameter-to-thickness ratio of 60. For BCPF-1, the welded end ring plate was 170 mm wide and 10 mm thick, and it projected 110 mm from the outside of the tube. For BCPF-2, the welded end ring plate was 120 mm wide and 10 mm thick, and it projected 10 mm from the outside of the tube and 104 mm from the inside of the tube. The size of the fillet welds was designed as 8 mm by one pass. The studs were 16 mm in diameter and 96 mm in length, and the spacing

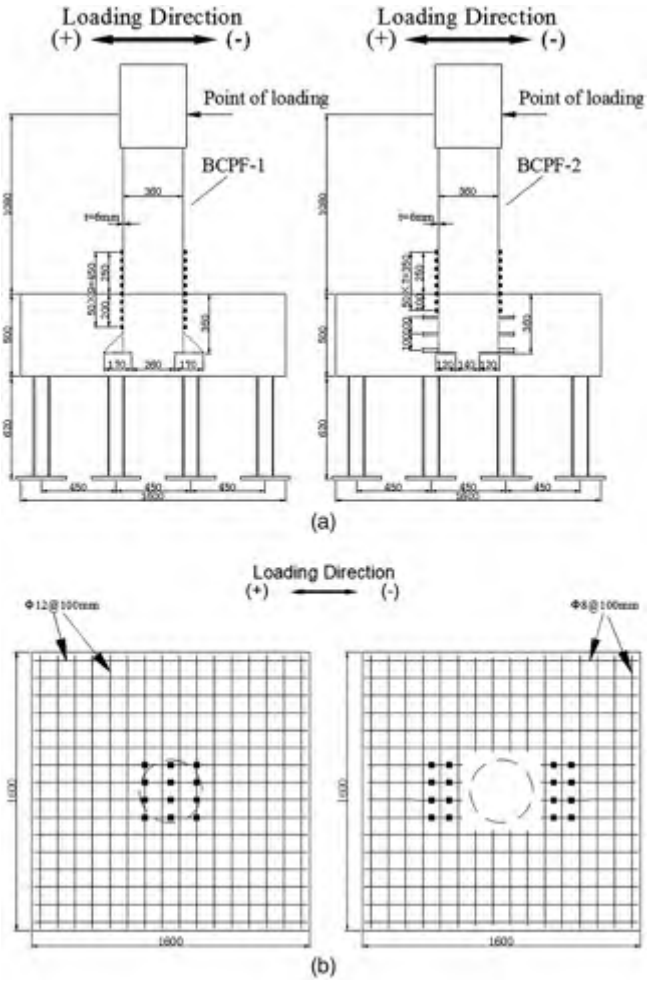

Fig. 2. Geometry and gauges of models

between two studs was approximately 100 mm. There were three rows of the studs, with 10 studs for each row, welded uniformly around the column bottom end. The model columns were tested as a vertical cantilever beam, with the point of loading located at 1,080 mm above the surface of the footing.

The dimensions of the model footing were 1,600 × 1,600 mm in plan and 500 mm deep, as shown in Figs. 2 and 3. For both models, the longitudinal reinforcement at the top of the footing consisted of 8-mm-diameter deformed bars spaced at 100 mm, and at the bottom of the footing 12 mm deformed bars were spaced at 100 mm in both directions parallel and perpendicular to the direction of the horizontal loading. The vertical reinforcement in the footing was 6-mm-diameter round J-shaped bars detailed with a 135° seismic hook at one end and a 90° hook at the other end. The vertical reinforcement was arranged at each intersection of the 8-mm-diameter top rebars, except in the column-footing joint region.

For each H-pile, four 14-mm-diameter deformed bars were welded to the web near its top end for anchorage into the footing. The anchor bars were aligned as close as possible to minimize the moment sustained by the pile-to-pile-footing connection. The section properties of the H-piles are shown in Fig. 3(a), and the pile layout is shown in Fig. 3(b). The pile length was taken as six times the pile width so that an inflection point could be observed in case the embedded top end of the pile bore some moment. The pile bottom end was bolted to H-steel beams that were fixed to the rigid reaction floor. The end condition of the piles might not fully

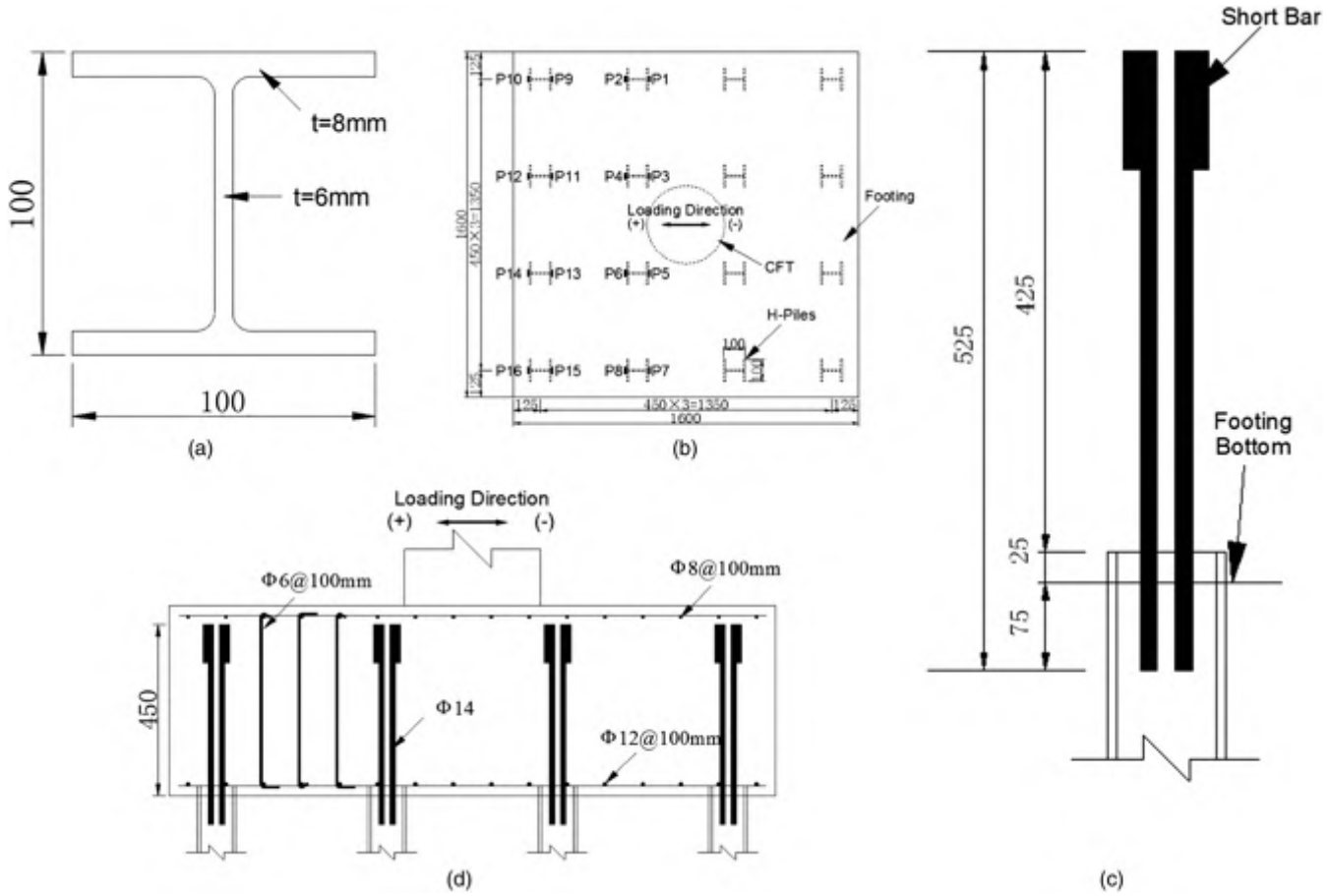

Fig. 3. Arrangement and detail of H-piles

Table 2. Material Properties

	Steel									
	Base plate (MPa)		Steel tube (MPa)		Pile flange (MPa)		Pile web (MPa)		Concrete f'_c (MPa)	
Model	f_y	f_u	f_y	f_u	f_y	f_u	f_y	f_u	Footing	Column
BCPF-1	295	420	331	435	347	459	393	523	27.3	31.8
BCPF-2									27.5	29.4

Note: f_y = yield strength of steel; f_u = tensile strength of steel.

represent the flexibility of piles in soil foundation; however, it allowed simplicity of testing with a relatively clear boundary condition.

Materials

The steel strengths shown in Table 2 are based on tensile tests of samples taken from the base plate of the column, the steel tube, and the flange and web of the steel H-piles. Ordinary cement and crushed rock aggregates with maximum size of 20 mm were used for the concrete. The concrete strength was determined based on compression tests of 200 mm concrete cubes as per the Chinese standard. The age of concrete at the model test day and material test day were 62 days and 65 days, respectively. The axial compressive strength of the concrete, f'_c, was calculated as 0.8 times the cubic strength f_{cu} in the following discussion. The steel for the reinforcement consisted of the Chinese Grade HRB335 steel bars with a specified yield strength, f_y, of 335 MPa, and the stud shear connectors consisted of HRB345 steel with a specified yield strength, f_y, of 345 MPa.

Construction of Models

The base plate and shear stud connectors were welded to the steel tubes for BCPF-1 and BCPF-2 by qualified welders following a standard procedure (Chinese Standard 2003, GB50017). Four rebars were welded to the web of each H-pile, as shown in Fig. 4(a). After the H-piles were prepared, 16 of them were fixed to the H-steel base beams, which were bolted to the strong reaction floor at the laboratory. A temporary support was built and the model footing steel cage was fabricated, as exhibited in Fig. 4(b). The so-called J-shaped reinforcement bars with a 135° seismic hook at one end and a 90° hook on the other end were used as vertical reinforcement. The seismic hooks of the stirrups were alternated from top to bottom for each consecutive spacing in each direction. When the erection of the tube was finished, the model construction was completed by pouring concrete into the footing and the column tube. After casting the concrete into the forms, the top surfaces of the footings were kept moist with wet burlaps for two weeks to avoid cracking. The forms were then removed and the model was air-dried until testing.

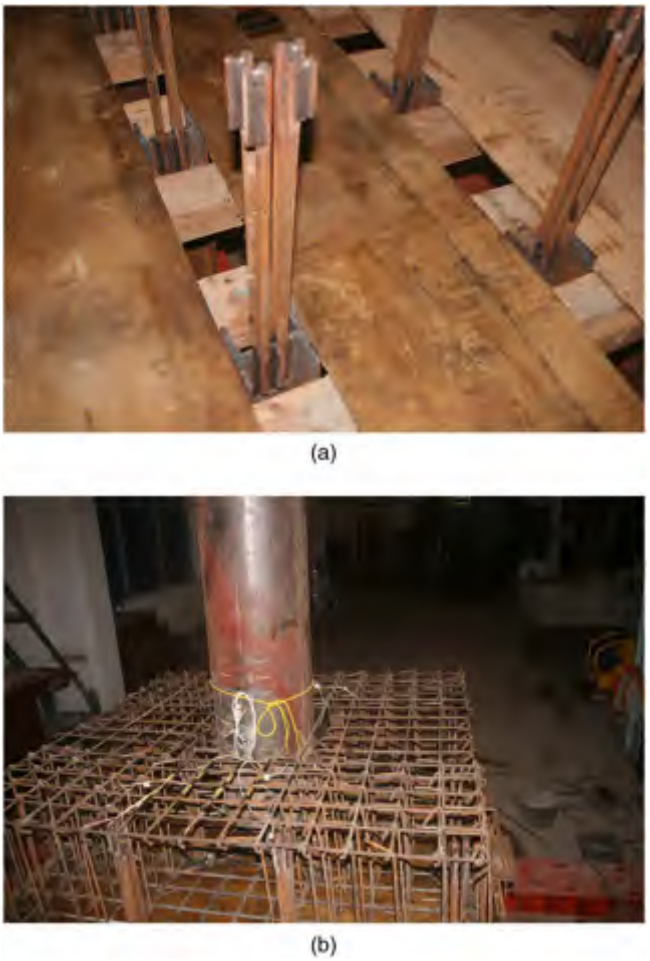

Fig. 4. (a) H-pile anchor bars; (b) footing steel cage (images by the authors)

Test Setup

The tests were performed using the test setup shown in Fig. 5. Cyclic horizontal forces were applied with a double-acting actuator. A constant axial load was applied by posttensioning two high-strength steel bars with pressure-controlled hydraulic center-hole jacks. Four H-shaped steel base beams were fixed to the rigid ground floor, and then the model was attached to the four H-shaped steel base beams with high-strength bolts.

The applied horizontal force was measured by calibrated load cells, and the applied vertical force was measured by means of a hydraulic gauge. As shown in Fig. 5, displacement at the application point of the horizontal force was measured by linear potentiometers. The rotation of the footing was measured by four linear potentiometers placed vertically, and the horizontal displacement of the footing was measured by linear potentiometers placed horizontally parallel to the loading direction in the middle of the footing. The sliding displacement of the H-steel base was also monitored by linear potentiometers at the end of the H-piles.

Uniaxial high-elongation strain gauges were placed along the height of the column and in the footing, as shown in Fig. 2(a), to monitor the longitudinal strain distributions in the steel tube below and above the footing surface. Footing reinforcement strain measurement was designed to monitor the behavior of the flexural reinforcement, with locations shown in Fig. 2(b). Strain gauges were also installed on the H-piles near the pile-to-pile-footing connection to assess the pile reactions under the footing, as indicated in Fig. 3(b).

Loading Program

The loading program attempted during the testing is shown in Fig. 6, which is based on ATC-24 (Applied Technology Council 1992). The model was first vertically posttensioned to 400 kN to simulate gravity load, then the model was subjected to a reversed cyclic lateral displacement history applied in a number of incremental steps. The peak of each loading cycle was controlled by displacement increment. Cyclic displacements were increased by multiples of the ductility factor μ (the ratio of peak displacement to yield displacement Δ_{my}). The yield displacement Δ_{my} is defined by the following Eq. (1):

$$\Delta_{my} = \Delta_{cy} + \Delta_{ry} + \Delta_{fy} \quad (1)$$

where Δ_{cy} and Δ_{ry} = displacements attributable to column deformation and footing rotation at yielding of the CFT column; and Δ_{fy} = displacement in the middle of footing at yield of the column. Nonlinear analysis by a Fortran program was used to estimate the yield displacement, and Δ_{my} was computed as 8 mm. On the basis of concrete and steel characteristics, the relationship between moment and curvature can be obtained to calculate the yield displacement by the program. For the first three peak displacements before Δ_{my}, two full cycles of lateral loading were applied to the column; however, for the first three levels after Δ_{my} (including Δ_{my}), three full cycles of reversed lateral loading were applied. Thereafter, two full cycles of reversed lateral loading were applied for other levels of displacement, as shown in Fig. 6.

Experimental Results and Discussion

General Observations

BCPF-1. The column-footing model BCPF-1 behaved well during testing as the capacity rose steadily with increasing lateral displacement, and no evidence of severe damage could be seen in the footing throughout testing. A yield strength of 296.4 kN was attained at 20 mm lateral displacement, thereafter, the column capacity increased slowly. At 35 mm, cracks appeared at the pile-footing interface and extended into the footing; the width of the cracks increased with subsequent cycles at the same displacement level. The maximum horizontal load of 370.7 kN was reached during the first cycle to 50 mm, at this point the steel tube protruded at the column-end and diagonal cracking was initiated from the column base, and cracks on the face of the footing continued to expand upward, as shown in Fig. 7(b). At a lateral displacement of 60 mm, diagonal cracks formed at the pile-footing interface near the footing edges, as shown in Fig. 7(c), suggesting a block rupture may have initiated. After this stage, footing cracking ceased further development, following the formation of a full plastic hinge at the column end. Local buckling of the steel tube initiated at a lateral displacement of 75 mm, and when the displacement reached 95 mm, a fracture developed around the circumference of the tube, as shown in Fig. 7(a), corresponding to a sudden decrease in the peak strength. The model sustained limited damage to the footing, and the strain gauges installed on the H-piles indicated that there was no yielding.

BCPF-2. At the initial loading stage, the response of BCPF-2 was similar to BCPF-1. After achieving the horizontal yield force of 274 kN, the footing capacity rose marginally. During the first cycle to the peak lateral displacement of 35 mm, cracks initiated at the pile-footing interface and then extended into the side of the footing, as shown in Fig. 8. A maximum horizontal force of 358.4 kN was attained when the lateral displacement was increased to 50 mm. During the first cycle to the peak displacement of 50 mm

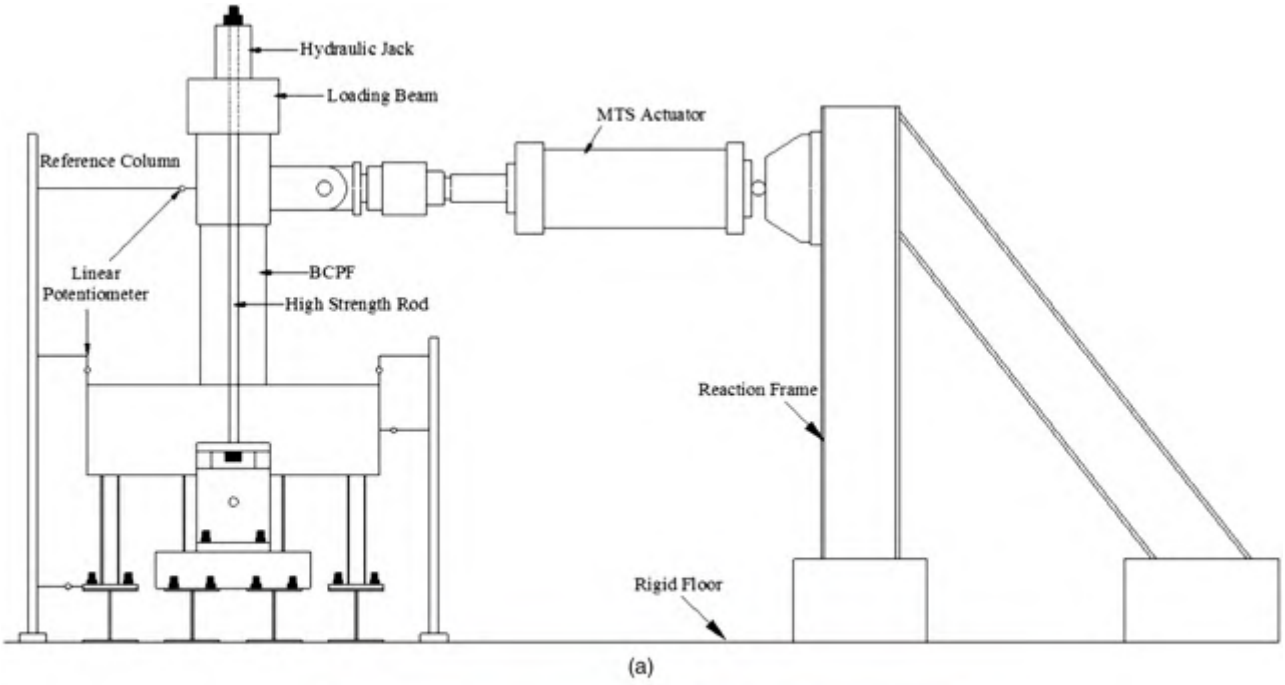

(a)

(b)

Fig. 5. Test setup and instrumentation (image by the authors)

in the reverse direction, slight buckling was observed at the base of column, and diagonal cracks formed near the base of column extending to the top of the footing. During the second cycle corresponding to a peak displacement of 74 mm, a large gap opened between the column and the foundation on the tension side, and pulverized concrete spilled out through the crack in the buckled region as the crack opened wider. The first cycle to 95 mm was completed, and then the test was stopped because of a significant fracture along the perimeter of the steel tube at the buckled region. The model had only limited damage to the footing, and as in the case of the specimen BCPF-1, no yielding occurred in the H-piles.

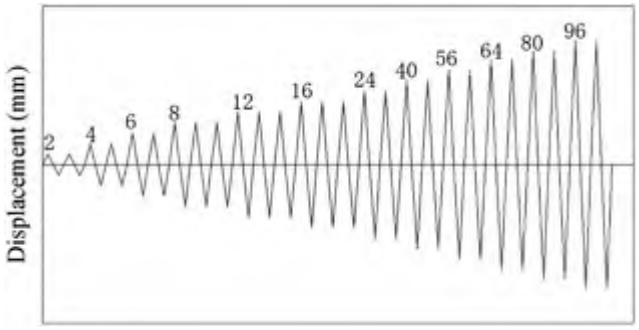

Fig. 6. Loading program

Horizontal Force-Displacement Response

The horizontal force-displacement hysteretic responses and the comparison of the envelops of the models are shown in Fig. 9. The measured horizontal forces were corrected by subtracting the horizontal component of the posttensioning forces measured for the high-strength steel rods for axial loading. As shown in Fig. 9, both models exhibited stable hysteretic responses, and the shapes of the hysteretic loops indicate reasonably satisfactory energy absorption. Both models showed an essentially linear response at the initial loading stage, and the yield point is reached at a total displacement of 20 mm. An additional increase in the load carrying capacity of the model was evident because of strain hardening of the tube steel, and the maximum applied horizontal force was reached at the first peak displacement of 50 mm. Thereafter, the load dropped following steel tube buckling; however, the models were able to sustain 80% of the maximum horizontal force corresponding to a peak displacement of 75 mm. Meanwhile, both specimens sustained limited damage to the footing, and testing was halted due to low-cycle fatigue fracture of the steel tube. This clearly suggests that the CFT column-to-footing connection details used in this research were effective.

Deformation Components

During testing of the models, the rotation of the footing was measured by two pairs of linear potentiometers, and the horizontal displacement of the footing was measured by a linear potentiometer at the middle of the footing. Thus, the components of the pier displacement due to footing rotation, Δ_r, and the horizontal displacement of the footing, Δ_f, can be separated from the measured total horizontal displacement, Δ_m. The difference between $\Delta_r + \Delta_f$ and Δ_m can be termed as the column deformation component, Δ_c, which corresponds to the displacement component attributable to deflection of the column. Fig. 10 compares different deformation components with the total lateral displacement. A structural ductility factor μ_c can be defined using Eq. (2) for describing the deformation capability of the model column:

$$\mu_c = \frac{\Delta_m - \Delta_r - \Delta_f}{\Delta_{my} - \Delta_{ry} - \Delta_{fy}} \tag{2}$$

where Δ_{my} = yield displacement obtained by the extrapolation of the measured yield displacement; and Δ_{ry} and Δ_{fy} = measured rotational displacement and horizontal displacement corresponding to Δ_{my}. Before the apparent load degradation, a maximum column ductility factor of approximately $\mu_c = 5.3$ can be calculated for both model BCPF-1 and model BCPF-2.

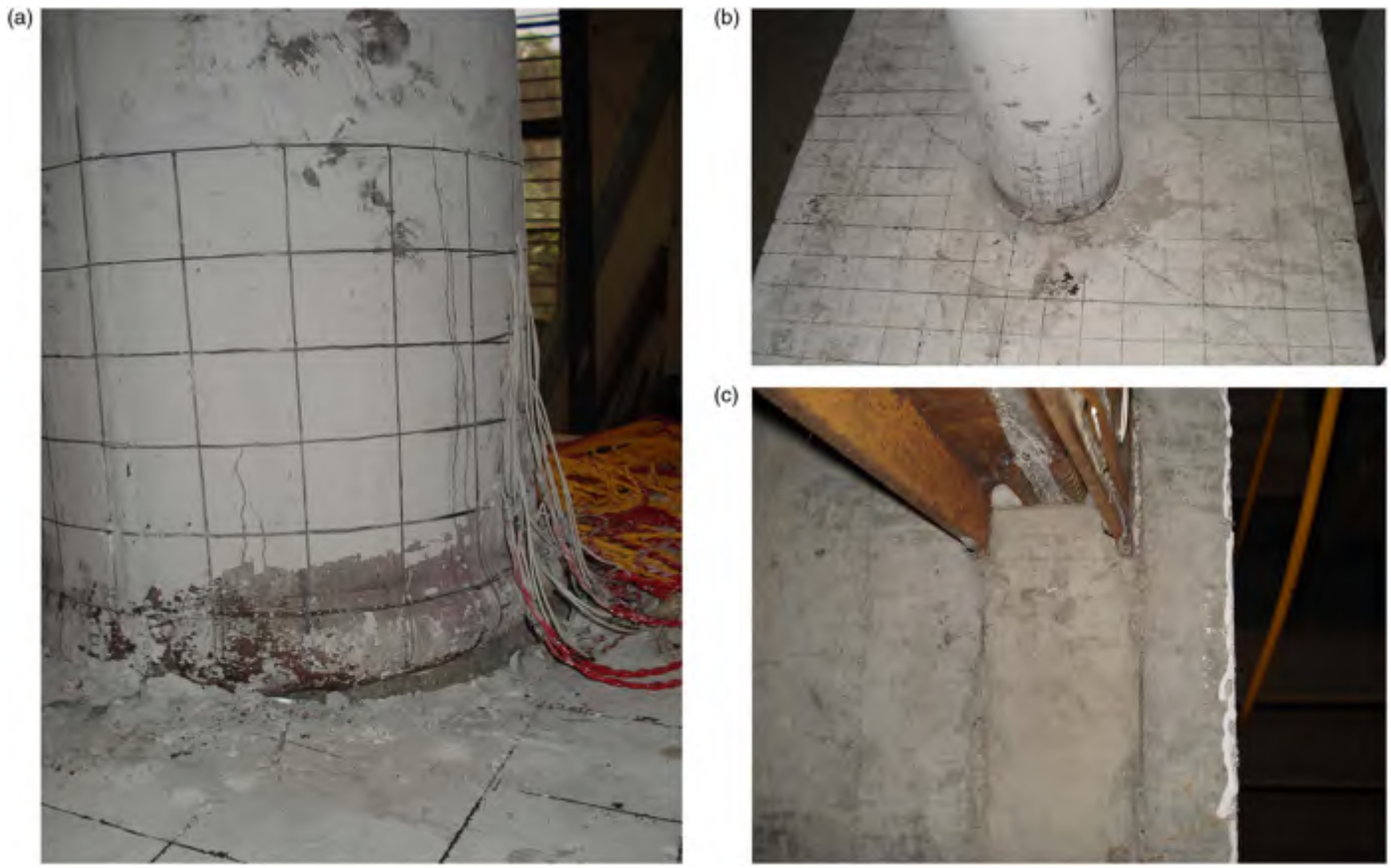

Fig. 7. Damage to model BCPF-1 (images by the authors)

(a)

(b)

(c)

Fig. 8. Damage to model BCPF-2 (images by the authors)

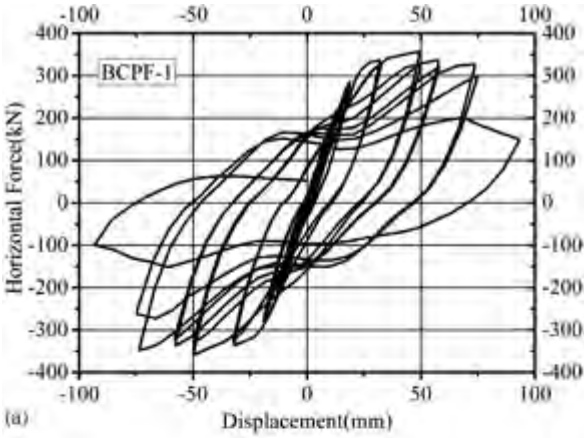

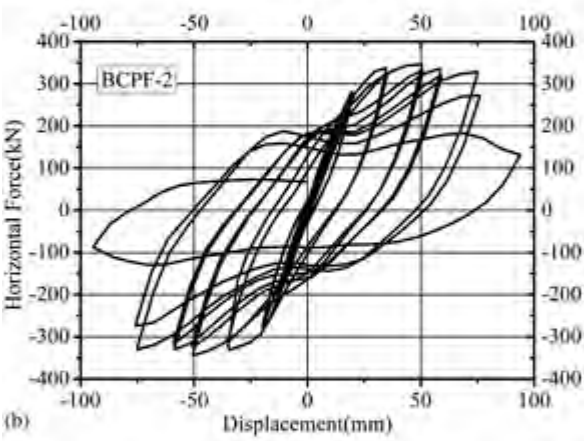

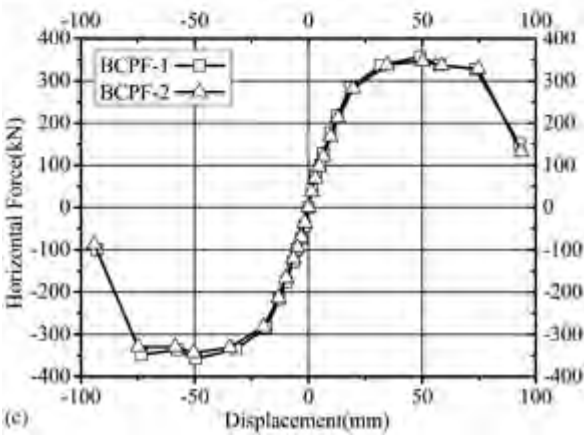

Fig. 9. Cyclic force-displacement response of models: (a) BCPF-1; (b) BCPF-2; (c) comparison of envelopes

Steel Tube Strains

Figs. 11(a) and 11(b) show the vertical distributions of strains in the steel tube on the tension side of the tube at the first loading peak in the push loading direction for BCPF-1 and BCPF-2, respectively. Positions of the strain gauges shown in Fig. 11 are related to the heights of the gauges above or below the footing surface. Vertical dashed lines in Fig. 11 show the yield strain of the steel tube. The strains on the tensile side of the steel tube are positive both inside and above the footing. Though not shown in Fig. 11 due to the scattering of the data beyond the lateral drift displacement of 12 mm, the strains of steel tube above the footing surface eventually all exceeded the steel yield strain.

Footing Longitudinal Reinforcement Strains

The footing flexural design was based on a critical section at the column face using the effective width proposed by Priestley and Seible (1991). Figs. 12(a) and 12(b) show the strains at the first loading peaks of a top longitudinal bar in the footing and that of a bottom bar, respectively. Positions of the strain gauges are related to the distance from the footing center line parallel to the loading axis. Dashed lines in Fig. 12 show the yield strain of the steel bar. As shown in Fig. 12, tensile strains are developed along the top and bottom bars in both the push and the pull directions. For the bottom

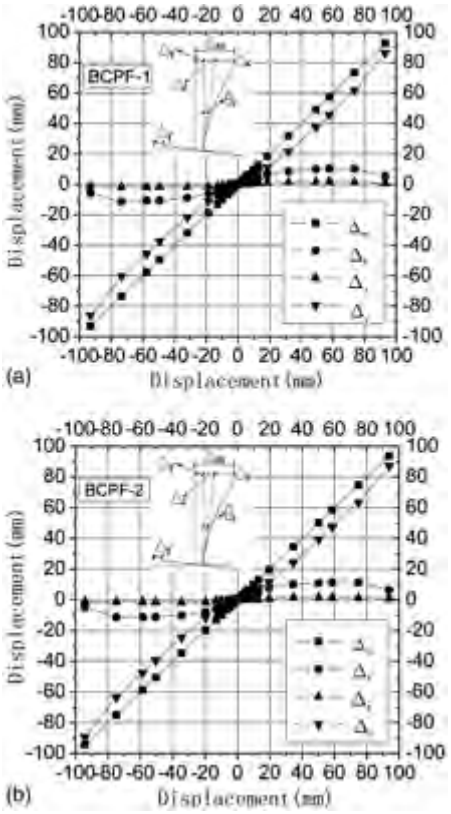

Fig. 10. Displacement components of models: (a) BCPF-1; (b) BCPF-2

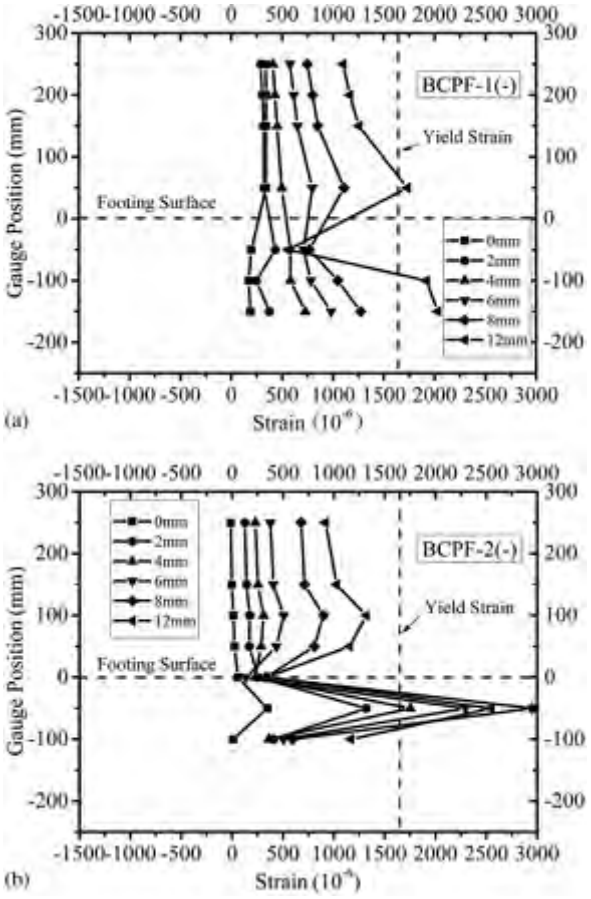

Fig. 11. Strain distributions of steel tubes: (a) Specimen BCPF-1; (b) Specimen BCPF-2

bars, the strains are small at the initial loading stage, but the strains increase rapidly in the subsequent loading levels. All the longitudinal bar strains are either less than or marginally larger than the yield strain, even at the final loading stages, suggesting that the use of effective width in design is conservative.

H-Piles Strain

Fig. 13 shows the strain distribution in the H-piles at the first loading peak in the push direction. Positions of the strain gauges are related to the distance from the footing centerline along the loading axis. As shown in Fig. 13, the strains at different positions are almost the same at the initial loading stage; however, after the horizontal displacement exceeds 8 mm, the strains closer to the footing centerline are larger than those of the outside piles, indicating that piles located closer to the center bore greater forces. The strain measurements also indicated that the strains on the two flanges of the pile had different responses, indicating the pile ends were subjected to bending. As an example, based on the measured strains at the horizontal displacement of 80 mm, the calculated bending moments and the axial forces are illustrated in Fig. 14. As shown in Fig. 14, despite the relatively large discrepancy between the data of the two model specimens, it is clear that the forces were larger in piles closer to the column centerline, along which the lateral force was applied, compared with the piles away from the column centerline. According to a previous analytical study by Duan and McBride (1995), when the length-to-thickness ratio of the footing cantilever measured from the column critical face is less than or equal to 2.2, the footing can be regarded as rigid. However, even though the length-to-thickness ratio of the footing cantilever in the current study was 1.24, the pile strain differences and thus force differences could still be observed for piles at different locations from the loading center line. Such shear lag effects might be attributable to the relatively rigidly fixed ends of the piles on the reaction floor. It is recognized that future experimental studies should be directed toward simulating the realistic stiffness of piles.

Discussion of Column-Footing Shear and Joint-Shear-Resisting Mechanism

The strut-and-tie modeling approach (Xiao et al. 1996, 1999) was considered for the design of the column footing in this study. The assumed strut-and-tie model used in the design is shown in Fig. 15. The applied force inputs to the footing corresponding to the ultimate moment of the column critical section are the resultant tensile force, T_c, resultant compressive force, C_c, and the shear force, V_c. The resultant tensile force, T_c, is transferred to the footing and resisted by three struts, C_1, C_2, and C_3. Tie T_4 is assumed to be equal to the tensile pile force, T_{p2}. Strut C_1 is equilibrated by Ties T_2, T_5, and T_6, provided by vertical stirrups and top reinforcement mat. Strut C_2 is equilibrated by Ties T_2, T_8 and T_{11}, which are also provided by vertical stirrups and the top reinforcement mat. Struts C_1, C_2, and C_3 and T_1 are balanced horizontally at their intersection with the resultant tensile force, T_c. On the compressive side of the footing, the resultant compressive force C_c, subtracted by C_6, is resisted by C_3 and C_8, and the shear force V_c, along with the horizontal component of C_3, is resisted by T_5 and the horizontal component of C_8. The configurations of the struts and ties are established based on the application lines of the applied forces and resistant forces and may vary for different column footings.

The vertical Ties T_2 and T_3 must be resisted by the shear-resisting mechanisms of the footing concrete and vertical stirrups.

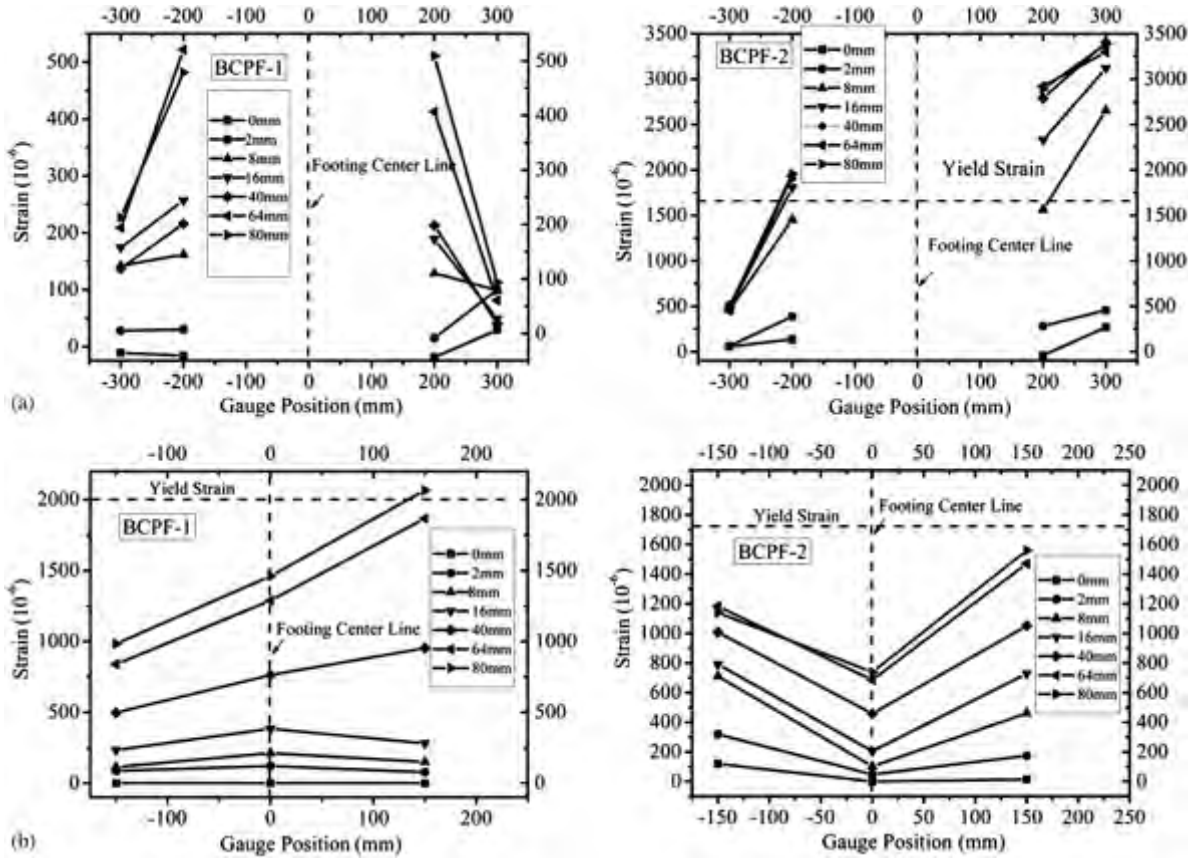

Fig. 12. Distributions of footing longitudinal steel strains: (a) top steel mat; (b) bottom steel mat

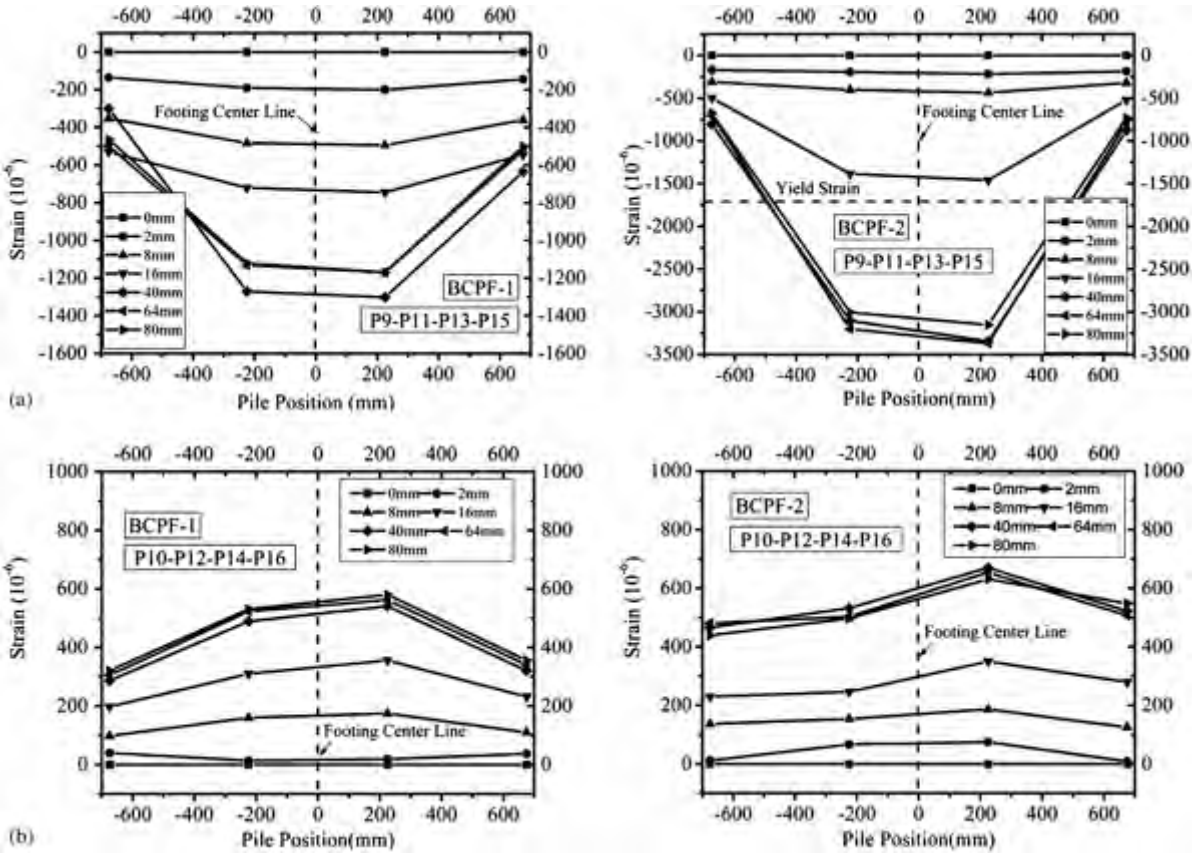

Fig. 13. Strain distributions of H-piles: (a) compression side; (b) tension side

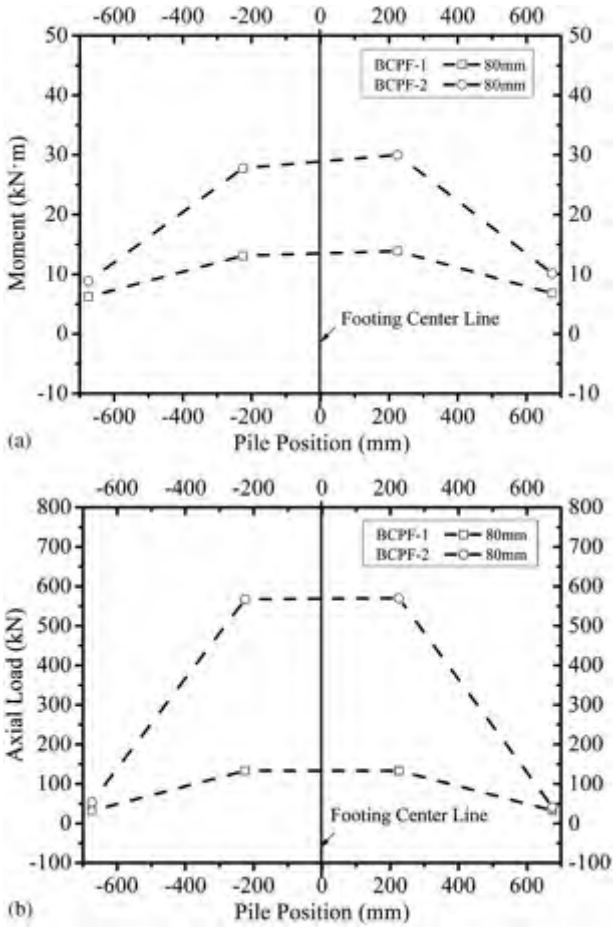

Fig. 14. Distribution of estimated pile-end forces: (a) moment distribution; (b) axial load distribution

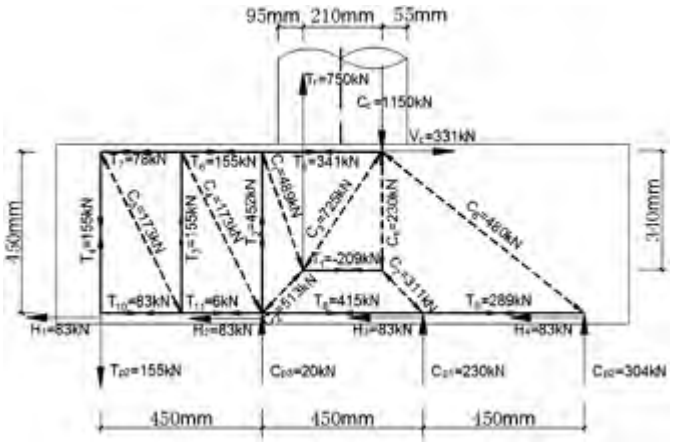

Fig. 15. Strut-and-tie analysis

Following the suggestions by Xiao et al. (1999), stirrups within an effective area are considered responsible to provide the resistance, V_{js}:

$$V_{js} = A_{\text{jeff}} \rho_{vs} f_y \tag{3}$$

where A_{jeff} = effective area in which the vertical stirrups resist the resultant tensile force, the forces in Ties T_2 and T_3, and can be defined based on a three-dimensional crack with 45° slope around the column tube in tension (Xiao et al. 1999); ρ_{vs} = ratio of the area of the footing vertical stirrups; and f_y = yield strength of the reinforcement. The depth of the crack (or the distance of the boundary of the shaded area to the boundary of the steel tube in tension) is assumed to be equal to the embedment depth, l_e. The depth of the crack reduces from l_e to zero linearly if the distance between the boundary and neutral axis reduces from $R(1+\cos\beta)$ to zero. Thus, A_{jeff} for the CFT column footing can be calculated as follows:

$$A_{\text{jeff}} = \int_{\beta}^{\pi} \left(R + l_e \frac{\cos\beta - \cos a}{1 + \cos\beta} \right)^2 d\alpha - (\pi - \beta) R^2 \tag{4}$$

where β = half of the central angle of the compressive zone α_0; R = radius of the steel tube; and l_e = embedment depth of the CFT column.

The calculated shear resistance V_{js} is larger than the required force $T_2 + T_3$, thus, it is verified that the footing was sufficiently reinforced against joint shear failure. In this analysis, concrete shear resisting mechanism is conservatively neglected.

Conclusions

Two column and pile-footing models, composed of concrete-filled steel tubes, reinforced concrete footing, and steel H-piles that simulate a bridge substructure, were tested. Both models were subjected to combined axial load and cyclic lateral forces and were shown to have excellent hysteretic response with sufficient footing capacity and ductility. Full plastic hinging was developed at the column end. Findings from the experimental work further indicate that

1. The ductility of the columns was satisfactory, with both columns reaching a drift ratio of approximately 6% before significant loss in moment capacity occurred as a result of rupture of steel tube of the CFT column. Stable hysteretic curves obtained from the tests showed good energy dissipation.
2. The column-to-footing connection details tested in this study were shown to be effective and capable ensuring the development of the full moment capacity of the concrete-filled steel columns.
3. Flexural design based on effective width and shear design based on a strut-and-tie model are shown to be conservative. At the end of the test, the footing damage was light, with only a few minor cracks noticed on the footing.
4. The steel H-pile-to-pile-footing connection worked well. Anchorage details using four bars welded to the web of the H-piles could develop the full-design ultimate tensile capacity.

Acknowledgments

The research described in this paper was carried out at the Center of Integrated Protection Research of Engineering Structures (CIPRES) of the China Ministry of Education Key Laboratory of Building Safety and Energy Efficiency under the support of Program for Changjiang Scholars and Innovative Research Team Project (IRT0619) and the Department of Transportation of Hunan Province. The research was also conducted as a collaborative research program between Hunan University, the University of Southern California, and the University of California at Davis. The research was also partially facilitated by an international exchange program managed by the Multidisciplinary Center for Earthquake Engineering Research (MCEER) at State University of New York in Buffalo.

References

Applied Technology Council (ATC). (1992). "Guidelines for cyclic seismic testing of components of steel structures." *ATC-24*, Redwood City, CA.

Chinese Standard. (2003). "Code for design of steel structures." *GB50017*, China Plan Press, Beijing (in Chinese).

Duan, L., and McBride, S. B. (1995). "The effects of cap stiffness on pile reactions." *Concr. Int.*, 17(1), 42–44.

Hitaka, T., Suita, K., Kato, M. (2003). "CFT column base design and practice in Japan." *Proc., Int Workshop on Steel and Concrete Composite Construction*, National Center for Research in Earthquake Engineering, Taipei, Taiwan, 291–290.

Hsu, H., and Lin, H. (2003). "Performance of concrete-filled tube base connections under repeated loading." *Proc., Int. Workshop on Steel and Concrete Composite Construction*, National Center for Research in Earthquake Engineering, Taipei, Taiwan, 291–299.

Kadoya, H.; Kawaguchi, J., and Morino, S. (2005). "Experimental study on strength and stiffness of bare type CFT column base with central reinforcing bars." *Composite Construction in Steel and Concrete V*, R. Leon and J. Lange, eds., ASCE, Reston, VA, 127–136.

Kingsley, A., Williams, T., Lehman, D., and Roeder, C. (2005). "Experimental investigation of column-to-footing connections for high-strength vanadium steel concrete filled tube construction." *Int. J. Steel Struct.*, 5, 377–387.

Marson, J., and Bruneau, M. (2004). "Cyclic testing of concrete-filled circular steel bridge piers having encased fixed-based detail." *J. Bridge Eng.*, 9(1), 14–23.

Mays, T. W., and Hill, T. E. (2006). "A simplified design procedure for steel H-piles in areas of high seismicity to include the effects of pile buckling." *Structures Congress 2006: Structural engineering and public safety*, ASCE, Reston, VA.

Priestley, M. J. N., and Seible, F. (1991). "Design of seismic retrofit measures of concrete bridges." *Seismic assessment and retrofit of bridges*, *Structural System Research Rep. No. SSRP-9/03*, Dept. of Applied Mechanics and Engineering Sciences, Univ. of California, San Diego, 197–250.

Shama, A. A., Marder, J. B., and Aref, A. J. (2002). "Seismic performance and retrofit of steel pile to concrete cap connections." *ACI Struct. J.*, 99 (1), 51–61.

Xiao, Y.; Priestley, M. J. N., and Seible, F. (1996). "Seismic assessment and retrofit of bridge column footings." *ACI Struct. J.*, 93(1), 79–94.

Xiao, Y., Priestley, M. J. N., and Seible, F. (1999). "Seismic performance of bridge footings designed to current standards." *Seismic response of concrete bridges*, *SP-187*, American Concrete Institute, Farmington Hills, MI, 131–157.

Xiao, Y., Wu, H., Yaprak, T. T., Martin, G. R., and Mander, J. B. (2006). "Experimental studies on seismic behavior of steel pile-to-pile-cap connections." *J. Bridge Eng.*, 11(2), 151–159.